

# Reversible O–O Bond Scission and O<sub>2</sub> Evolution at MOF-Supported Tetramanganese Clusters

Xin He,<sup>§</sup> Andrei Iliescu,<sup>§</sup> Tzuhsiung Yang, Maxx Q. Arguilla, Tianyang Chen, Heather J. Kulik, and Mircea Dinca<sup>\*†</sup>



Cite This: <https://doi.org/10.1021/jacs.3c05374>



Read Online

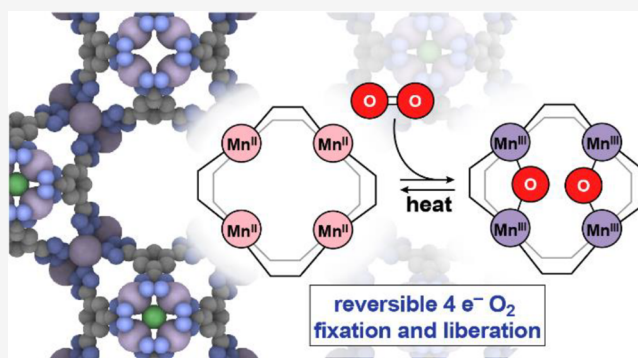
ACCESS |

Metrics & More

Article Recommendations

Supporting Information

**ABSTRACT:** The scission of the O–O bond in O<sub>2</sub> during respiration and the formation of the O–O bond during photosynthesis are the engines of aerobic life. Likewise, the reduction of O<sub>2</sub> and the oxidation of reduced oxygen species to form O<sub>2</sub> are indispensable components for emerging renewable technologies, including energy storage and conversion, yet discrete molecule-like systems that promote these fundamental reactions are rare. Herein, we report a square-planar tetramanganese cluster formed by self-assembly within a metal–organic framework that reversibly reduces O<sub>2</sub> by four electrons, facilitating the interconversion between molecular O<sub>2</sub> and metal-oxo species. The tetranuclear cluster spontaneously cleaves the O–O bond of O<sub>2</sub> at room temperature to generate a tetramanganese-bis( $\mu_2$ -oxo) species, which, in turn, is competent for O–O bond reformation and O<sub>2</sub> evolution at elevated temperatures, enabled by the head-to-head orientation of two oxo species. This study demonstrates the viability of four-electron interconversion between molecular O<sub>2</sub> and metal-oxo species and highlights the importance of site isolation for achieving multi-electron chemistry at polynuclear metal clusters.



## INTRODUCTION

Storing and unleashing the energy contained within the O<sub>2</sub> molecule requires control over the formation and scission of the four-electron double bond between two oxygen atoms.<sup>1–4</sup> Nature performs these demanding multi-electron transformations by distributing the redox burden among multiple metal ions: evolution created metalloenzymes with polynuclear clusters wherein metal ions act in concert to deliver or accept multiple electrons. Most relevant in this sense are the tetramanganese-calcium (Mn<sub>4</sub>CaO<sub>5</sub>) cluster in the oxygen-evolving complex (OEC) of photosystem II,<sup>1</sup> responsible for O<sub>2</sub> formation, and the tricopper clusters in multi-copper oxidases, which mediate O<sub>2</sub> reduction.<sup>2</sup> The critical step in both O<sub>2</sub> reduction and O<sub>2</sub> evolution is the interconversion between multinuclear metal-oxo species, where the O atoms carry formal –2 charges, and O–O bonded species where the oxygen atoms are more oxidized.<sup>5,6</sup> Attempts to mimic the natural systems with synthetic analogs have led to a number of elegant molecular clusters that shed light on the electron transfer events and stepwise mechanism of O–O bond cleavage and formation.<sup>7–19</sup> To our knowledge, however, the interconversion between molecular O<sub>2</sub> and metal-oxo species in either synthetic or enzymatic discrete systems has not been documented.

Multinuclear Mn clusters are particularly attractive as potential open sites for realizing multi-electron O<sub>2</sub> chemistry. In their reduced state, the manganese atoms provide multiple reducing equivalents and binding sites for oxygen reduction, reminiscent of multi-copper oxidases (MCOs) and cytochrome C oxidase,<sup>2,20</sup> which bind and reduce O<sub>2</sub> in an electron-rich “pocket” featuring multiple redox-active open sites. Similarly, in OEC of photosystem II, the Mn<sub>4</sub>Ca cluster provides not just multiple oxidizing equivalents but also four independent O-binding sites. Synthesizing molecular mimics capable of four-electron redox chemistry, which also provide multiple inward-oriented open metal sites for oxygen binding, as would be required for O–O coupling reactivity, has been difficult.<sup>13,14,21,22</sup> Furthermore, molecular mimics operating in solution are challenged by deleterious H-atom abstraction reactions that compete with the bimolecular coupling of terminal or bridging oxo species that would give rise to O<sub>2</sub>. We sought to circumvent these issues by exploiting the site-

Received: May 23, 2023

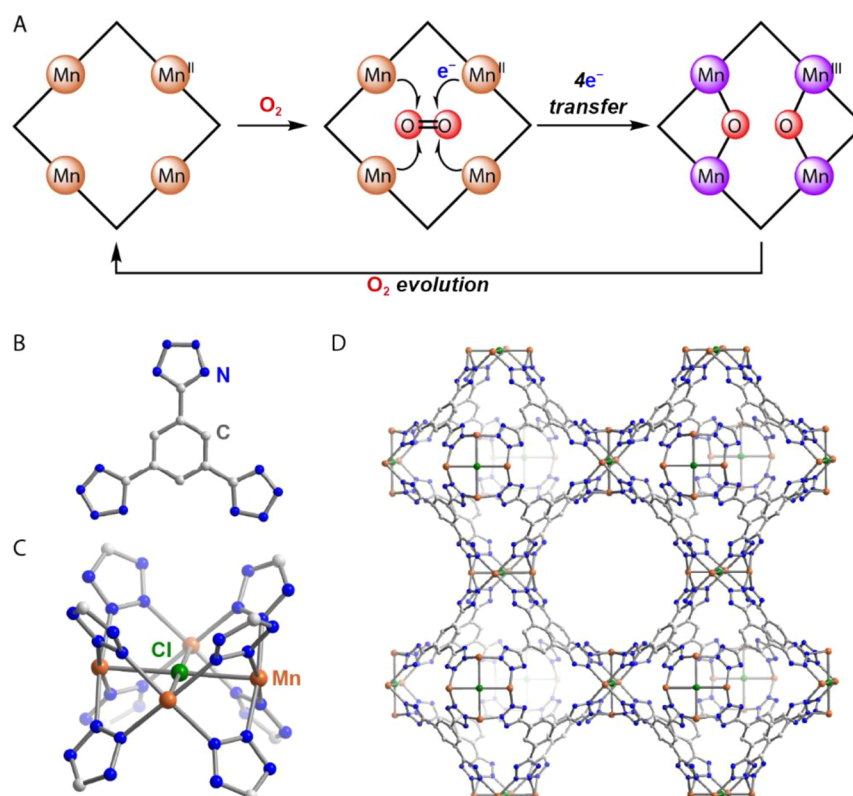


**Figure 1.** O<sub>2</sub> fixation and evolution at a site-isolated tetramanganese cluster with open metal sites. (a) Schematic representation of oxygen reduction and evolution through the intermediacy of bridging oxo species. (b) Structure of the BTT<sup>3-</sup> ligand. (c) Secondary building unit (SBU) of MnMnBTT is formed by a [Mn<sub>4</sub>Cl]<sup>7+</sup> core and eight bridging tetrazolate rings. (d) Crystal structure of MnMnBTT. Hydrogen atoms, solvent molecules, and charge-balancing extraframework Mn atoms are omitted for clarity.

isolation and potential for multi-electron chemistry of MOFs with multi-nuclear secondary-building units (SBUs).<sup>23</sup> The porous nature of MOFs enables solid–gas reactivity and flow chemistry without interference from solvent molecules, while the inherent site isolation of SBUs prevents intermolecular decay pathways. Functionally, this behavior is not unlike that of metalloenzymes, where the protein complex allows access of only specific molecules to the active site, and evidently also prevents active sites from reacting with each other. One material that provides many of the features we identified as necessary for multi-electron O<sub>2</sub> reactivity is Mn<sub>3</sub>[(Mn<sub>4</sub>Cl)<sub>3</sub>BTT<sub>8</sub>]<sub>2</sub> (MnMnBTT, **1**, BTT = 1,3,5-benzenetris-tetrazolate).<sup>24</sup> This MOF is made from BTT-bridged [Mn<sub>4</sub>Cl]<sup>7+</sup> SBUs wherein Mn<sup>2+</sup> ions sit in a square-planar arrangement and are bridged by a weakly coordinated chloride (Cl⋯Mn distance = 2.6725(10) Å) (Figure 1b–d). We hypothesized that removal of the central chloride anion would generate four inward-oriented open metal sites that would be primed for interacting with small molecules. Owing to their robust redox chemistry, the Mn atoms could thus engage particularly well with redox-active small molecules such as O<sub>2</sub> (Figure 1a).

## RESULTS AND DISCUSSION

**Synthesis and Characterization.** Soaking as-synthesized crystals of **1** in methanol for two weeks generates a crystalline material with the general formula Mn<sub>2.61</sub>[(Mn<sub>4</sub>Cl<sub>0.87</sub>)<sub>3</sub>BTT<sub>8</sub>]<sub>2</sub> (**2**), where on average, 13% of all SBUs are chloride-deficient. The partial removal of chloride from within the Mn<sub>4</sub>Cl SBUs thus creates chloride-free, neutral Mn<sub>4</sub>(tetrazolate)<sub>8</sub> clusters

that now account for approximately 13% among all SBUs in **2** (Figure 2a). Chloride removal is kept charge-neutral by the concurrent loss of extraframework, loosely bound Mn<sup>2+</sup> cations, according to the balanced SBU-based equation Mn[(Mn<sub>4</sub>Cl)(tetrazolate)<sub>8</sub>]<sub>2</sub> → 2 (Mn<sub>4</sub>)(tetrazolate)<sub>8</sub> + MnCl<sub>2</sub>. Prolonged methanol soaking for up to an additional two weeks did not facilitate further MnCl<sub>2</sub> removal from **2**. Activation of **2** by heating at 120 °C under dynamic vacuum removes most solvent molecules and thus generates a material with Mn<sub>4</sub> clusters that are free of both solvent and chloride. The amount of MnCl<sub>2</sub> “leached” out of **1** to produce **2** was confirmed by a combination of X-ray photoelectron spectroscopy (XPS), ion chromatography (IC), and inductively-coupled plasma mass spectrometry (ICP-MS) (Figures 2b, S1–S4 and Table S1). Formation of AgCl precipitate upon addition of AgBF<sub>4</sub> to the methanolic filtrate collected after MnCl<sub>2</sub> elimination confirmed the leaching of chloride anions from MOF SBUs (Figure S5). Compound **2** retains crystallinity and porosity after the soaking process, as confirmed by powder X-ray diffraction (PXRD, Figure S6) and an N<sub>2</sub> adsorption isotherm, which gave an apparent BET surface area of 2301 m<sup>2</sup>/g (Figure S7), slightly larger than the parent material.<sup>24</sup>

Treatment of **2** with dry O<sub>2</sub> under strictly moisture-free conditions at room temperature yields dark-brown crystals of MnMnBTT-O (**3**, Figures 2b and S8). Compound **3** exhibits broad absorption in the visible and near-infrared range (λ<sub>max</sub> = 464 nm), contrasting with **2**, which shows negligible absorption in these regions, as would be expected for Mn<sup>II</sup> compounds. The strong electronic absorption in **3** is clearly

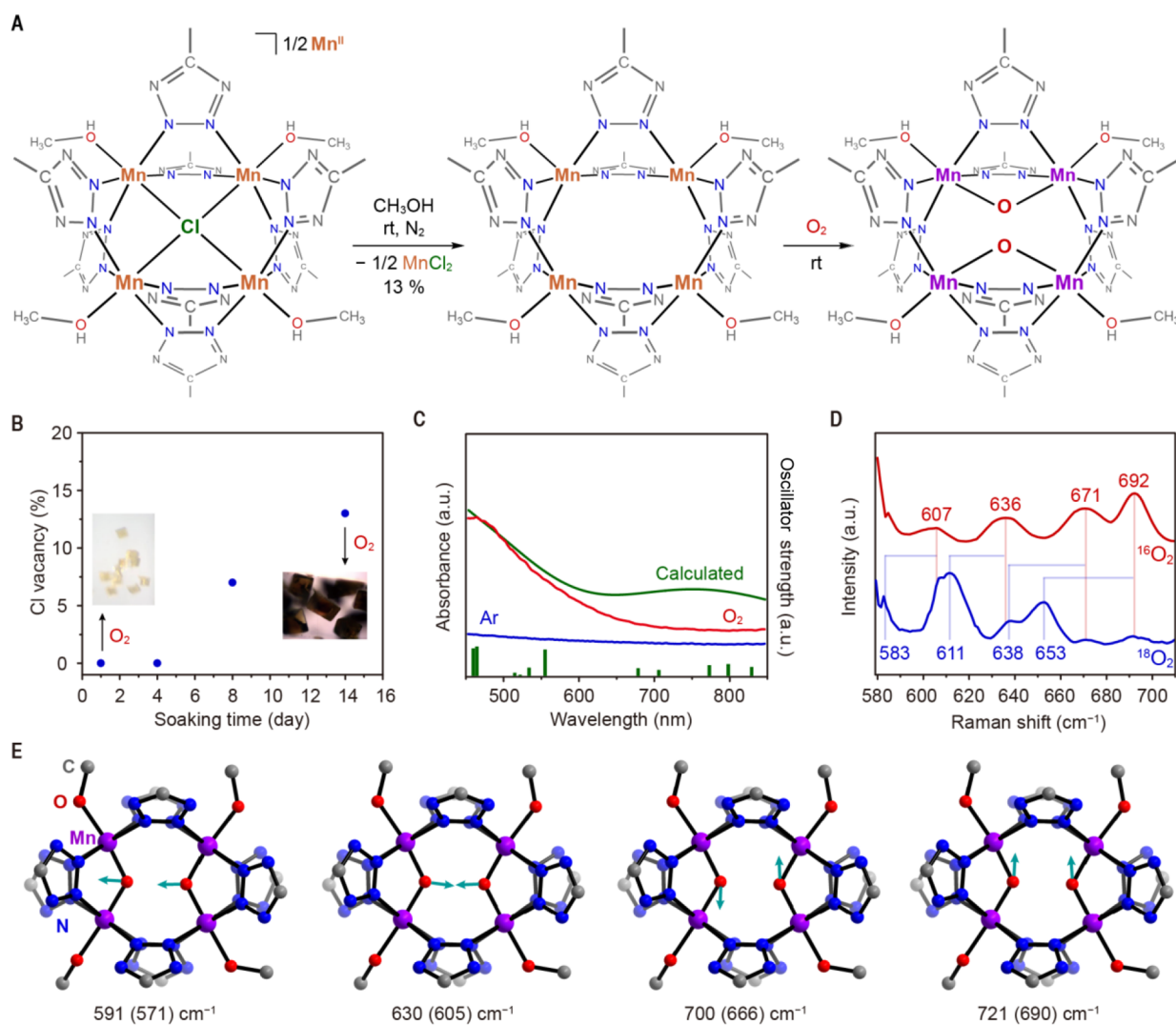


**Figure 2.** Generation of vacant tetramanganese sites and oxygen reduction reactivity. (a) Generation of tetramanganese open sites and their O<sub>2</sub> reduction reactivity. (b) Average chloride vacancy in each SBU determined by XPS, as a function of methanol soaking time. Insets show the color of activated, O<sub>2</sub>-exposed samples that were soaked in methanol for 1 day and 14 days, respectively. (c) Experimental electronic absorption spectra of activated **2** (blue trace) and **3** (red trace), and calculated electronic adsorption spectra of **3** (green trace), along with calculated individual excitations (green bars). (d) Raman spectra of **3**-<sup>16</sup>O and **3**-<sup>18</sup>O. (e) Simulated vibrational modes and corresponding frequencies for the [Mn<sub>4</sub>(μ-oxo)<sub>2</sub>(tetrazole)<sub>8</sub>(CH<sub>3</sub>OH)<sub>4</sub>] unit. Vibrational frequencies for <sup>18</sup>O models are shown in parentheses.

indicative of oxidation at the Mn sites (Figures 2c and S9–S12). Importantly, crystals of **1** that lack chloride vacancies do not show any visible changes upon exposure to O<sub>2</sub>, suggesting that only those Mn<sub>4</sub> clusters that have internal open coordination sites produced by chloride elimination are responsible for O<sub>2</sub> reactivity (Figure 2a). A Raman spectrum of **3** shows four bands at 607, 636, 671, and 692 cm<sup>-1</sup> (Figure 2d). These bands are significantly lower in energy than the reported ν<sub>O–O</sub> frequencies for Mn(III)-peroxo (819–885 cm<sup>-1</sup>) and Mn(III)-superoxo (1124 cm<sup>-1</sup>) compounds, ruling out the formation of peroxo or superoxo species in **3**.<sup>25–27</sup> More in line with the vibrational features in **3** are bis(μ-oxo) dimanganese units,<sup>28</sup> which display a multitude of peaks between 600 and 700 cm<sup>-1</sup>, pointing to full O–O bond cleavage and the formation of μ-oxo in **3**. <sup>18</sup>O-labeling studies revealed that the low-frequency Raman bands are all isotopically sensitive: upon treatment of **2** with <sup>18</sup>O<sub>2</sub>, all four Raman bands shifts to 583, 611, 638 and 653 cm<sup>-1</sup>, respectively (Figures 2d and S13). Corroborating the

formation of bis(μ-oxo) dimanganese units in the vacant Mn<sub>4</sub> clusters are density functional theory (DFT) calculations. Structural optimization and analysis of a truncated model cluster built from four Mn ions, two oxygen atoms, eight tetrazole rings, and four methanol molecules coordinated exo to each Mn ion (Figure 2e) indicates all manganese ions are in the +III formal oxidation state, as would be expected for a cooperative four-electron reduction of O<sub>2</sub> (Figures 2e and S9). The computed vibrational frequency analysis gives four scaled vibrational modes at 591, 630, 700, and 721 cm<sup>-1</sup>, which shift to 571, 605, 666, and 690 cm<sup>-1</sup> for the <sup>18</sup>O model, in excellent agreement with the experimental Raman bands assigned to the dimanganese μ-oxo species (Figures 2e and S14). Notably, computational models involving incomplete O–O bond cleavage, that is, the formation of dioxygen, superoxo, or peroxo species, gave vibrational frequencies of 1455, 1243, and 883 cm<sup>-1</sup>, respectively, for the O–O stretch (Figures S15–S19), which are not observed in **3**. The combined experimental and computational results establish the molecular formula of **3**



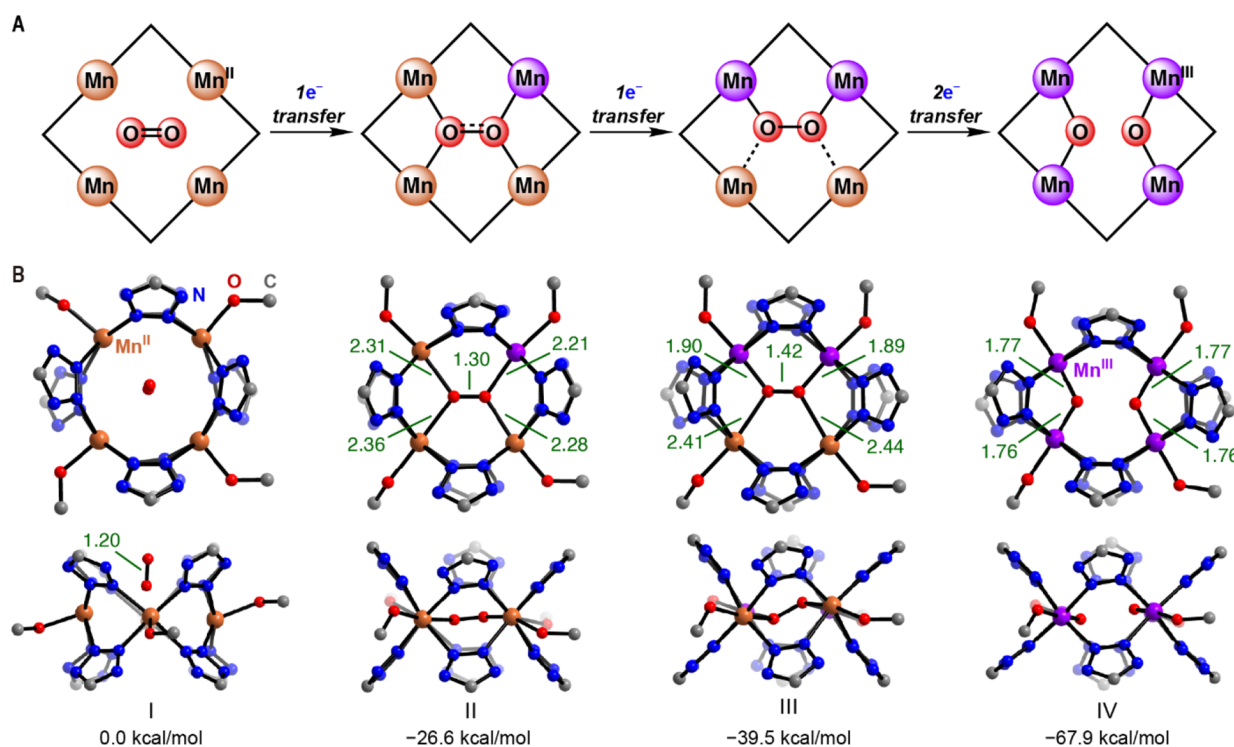


**Figure 3.** Calculated reaction pathway for O<sub>2</sub> reduction and evolution at a tetramanganese site and free energies of reaction intermediates. (a) Electron transfer sequence along the oxygen reduction (from left to right) and evolution (from right to left). (b) Optimized structures shown normal and parallel to the plane formed by the four Mn ions in a Mn<sub>4</sub> cluster, with the associated free energy for the following: (I) native all-Mn<sup>II</sup> cluster with O<sub>2</sub>; (II) superoxo intermediate; (III) peroxy intermediate; and (IV) all-Mn<sup>III</sup> di-μ<sub>2</sub>-oxo cluster. Hydrogen atoms are omitted. All distances are reported in Å.

as Mn<sub>2.61</sub>[(Mn<sub>4</sub>Cl)<sub>2.61</sub>(Mn<sub>4</sub>(μ<sub>2</sub>-O)<sub>2</sub>)<sub>0.39</sub>BTT<sub>8</sub>]<sub>2</sub>, whereby the “empty” or neutral Mn<sup>II</sup><sub>4</sub> clusters in **2** (13% of all SBUs, vide supra) undergo four-electron oxidation overall to quantitatively yield corresponding Mn<sup>III</sup><sub>4</sub>(μ<sub>2</sub>-O)<sub>2</sub> clusters in **3**.

#### Calculated Reaction Pathway for O<sub>2</sub> Reduction.

Computational analysis provided a reasonable reaction pathway and intermediates during the scission of the O–O bond (Figure 3). The first one-electron reduction of O<sub>2</sub> by the Mn<sub>4</sub> cluster gives a μ<sub>2</sub>-η<sup>2</sup>,η<sup>2</sup> superoxo intermediate II wherein one Mn<sup>II</sup> is oxidized to Mn<sup>III</sup> and the O–O bond is elongated to 1.30 Å, compared to 1.20 Å in free O<sub>2</sub>, slightly longer than that of a reported monomeric end-on Mn<sup>III</sup>-superoxo (1.249(4) Å).<sup>26</sup> The second 1e<sup>-</sup> transfer from an adjacent Mn<sup>II</sup> to the superoxide species has a barrier of 1.2 kcal/mol and affords a trans-μ-1,2-peroxy intermediate III bearing a di-Mn<sup>III</sup> unit (Table S2 and Figure S20). In intermediate III, the Mn<sup>III</sup>–O bonds are approximately 0.5 Å shorter than the other two Mn<sup>II</sup>–O bonds. The Mn<sup>II</sup> can therefore be thought of as Lewis acids that weakly coordinate the peroxide thus activating it for further electron transfer. The O–O bond in III is further elongated to 1.42 Å, and is comparable to those found in binuclear Mn<sup>III</sup>-peroxy species, 1.452(5) Å,<sup>27</sup> and mononuclear side-on Mn<sup>IV</sup>-peroxy species, 1.415(2) Å.<sup>29</sup> Even though the final two-electron reduction of III to IV has a calculated barrier of 16.0 kcal/mol, it is exergonic by 28.4 kcal/mol and leads to the complete cleavage of the O–O bond, with the formation of the all-Mn<sup>III</sup> [Mn<sub>4</sub>(μ<sub>2</sub>-O)<sub>2</sub>] core (species IV in Figure 3) that is experimentally found in **3** (Table S2 and Figure S21). The tetramanganese core in IV deviates significantly from the original ~3.8 × 3.8 Å square shape to form a rectangle with approximate sides of 4.0 × 3.1 Å,

wherein the O⋯O distance between the two μ-oxo units is 2.42 Å.

**O<sub>2</sub> Evolution.** In **3**, O<sub>2</sub> is reduced by four electrons at the Mn<sub>4</sub> cluster to give [Mn<sup>III</sup><sub>4</sub>(μ<sub>2</sub>-O)<sub>2</sub>(tetrazole)<sub>8</sub>] units, as determined based on spectroscopic characterizations and density-functional theory (DFT) calculations (Figure 2, vide supra). Previous reports of multielectron activation of O<sub>2</sub> typically involve trinuclear clusters;<sup>13,14</sup> our strategy here represents an alternative involving tetranuclear clusters. Given the proximity and orientation of the two oxo groups within oxidized clusters in **3**, we envisioned a scenario where these groups could indeed couple to reversibly form an O–O bond and potentially even release O<sub>2</sub>. To probe this scenario, we monitored O<sub>2</sub> generation using real-time in-line mass spectrometry (MS), following counts for species with a mass-to-charge ratio (*m/z*) of 32, for <sup>16</sup>O<sub>2</sub>. However, *m/z* = 32 also corresponds to methanol, traces of which are released from the MOF at temperatures exceeding 65 °C, and which interferes with the <sup>16</sup>O<sub>2</sub> signal. Instead, we used <sup>18</sup>O<sub>2</sub> to produce and isolate <sup>18</sup>O-labeled **3**-<sup>18</sup>O. The labeled MOF was then evacuated and purged with He to remove any potential trace of left-over <sup>18</sup>O<sub>2</sub>. Gradually heating **3**-<sup>18</sup>O and monitoring the *m/z* = 36 MS signal produces a clear peak around 100 °C (Figure 4), which can only be assigned to <sup>18</sup>O<sub>2</sub>. In a control experiment, heating of **3** up to 150 °C under a flow of He gives no detectable signal for *m/z* = 36. Following the <sup>18</sup>O<sub>2</sub> evacuation from **3**-<sup>18</sup>O, the reduction of the Mn(III) centers in the material was corroborated by the change in color from dark-brown back to colorless, and the formation of a material spectroscopically indistinguishable from **2**. PXRD confirmed that the framework remains crystalline after O<sub>2</sub> evolution.

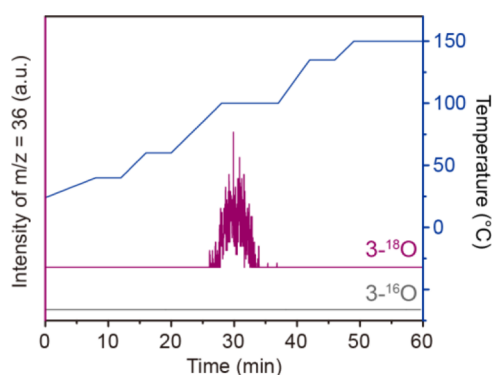


**Figure 4.** O<sub>2</sub> evolution from 3-<sup>18</sup>O. Oxygen evolution reactions were conducted in a continuous, tubular flow reactor under helium flow. The intensity of  $m/z = 36$  of the outlet gas was monitored using mass spectrometry.

Considering the rigid framework, intermolecular reaction pathways for O<sub>2</sub> formation can be ruled out. Likewise, O<sub>2</sub> formation by oxidation of solvent molecules is unlikely as none of the possible trace or guest solvent molecules are labeled with <sup>18</sup>O. Thus, we assign the observed  $m/z = 36$  signal to O<sub>2</sub> produced by coupling two bridging oxo groups in tetramanganese clusters.

The computational analysis in Figure 3 illustrates the reaction pathway for O<sub>2</sub> evolution. We note that the main driving force for O<sub>2</sub> evolution, which is endergonic, is the generation of gaseous O<sub>2</sub> in an open system. Starting from the manganese-oxide cluster, the first step is O–O bond formation via the interaction of two metal–oxo units. This step is particularly difficult and rarely observed in molecular systems, not least because the oxos require a radical character.<sup>6</sup> Notably, radical coupling and nucleophilic attack mechanisms for O<sub>2</sub> formation traditionally involve Mn<sup>IV</sup>-oxyl radical and/or Mn<sup>V</sup>-oxo electrophiles.<sup>11</sup> Similarly, in Nature, the OEC of photosystem II liberates O<sub>2</sub> via a tetra-manganese(IV) state of the Mn<sub>4</sub>CaO<sub>5</sub> cluster.<sup>1</sup> In our system, however, we show that high-valent manganese is not required for O<sub>2</sub> evolution in a tetramanganese cluster. Nonetheless, the calculated energy barrier for O–O bond formation, 44.4 kcal/mol, is relatively large. This observation can be attributed to the relatively low oxidation state of Mn in the MOF-supported, oxygen-evolving Mn<sup>III</sup><sub>4</sub>(μ<sub>2</sub>-O)<sub>2</sub> clusters, and may explain why O<sub>2</sub> generation from this system requires elevated temperature. Still, one important advantage of this MOF system is likely the favorable orientation of the two coupling oxo groups, which are fixed by the Mn<sub>4</sub> cluster in an entropically-favored conformation with a relatively short O...O distance of 2.42 Å. The subsequent steps are significantly less thermodynamically demanding, with O<sub>2</sub> release expected to be spontaneous upon forming the O–O bond. The last step, O<sub>2</sub> release, is essentially the reverse of a chemisorptive O<sub>2</sub> binding and is driven by running O<sub>2</sub> evolution in an open system under He flow. To our knowledge, this represents the first example of a discrete artificial Mn system that evolves O<sub>2</sub>.

**Activity of Related Mn<sub>3</sub>Ni Cluster.** The presence of four Mn atoms in the O<sub>2</sub>-evolving cluster in **3** allows one-electron redox processes at each Mn atom and raises the question of whether reactivity could be observed in the presence of just three Mn atoms. To test the necessity of all four Mn atoms, we targeted an isostructural trimanganese-mononickel cluster supported by the same tris-tetrazolate ligand. We had

previously shown that partially substituted clusters can be accessed by post-synthetic metal exchanges in the parent all-manganese MOF.<sup>30,31</sup> We focused on the Ni-exchanged clusters because the less oxophilic Ni<sup>2+</sup> is unlikely to allow oxidation to Ni<sup>3+</sup>, thereby potentially forcing one of the remaining Mn atoms to engage in multielectron chemistry. Furthermore, upon removal of central chloride ions from Mn<sub>3</sub>Ni clusters, Ni would adopt a favorable square-planar geometry. Thus, colorless crystals of **1** were soaked in a concentrated methanolic solution of anhydrous NiCl<sub>2</sub> at 50 °C for 18 h. The resulting green material, solvated **1-Ni**, remains crystalline and preserves the topology of the starting material, as confirmed by PXRD (Figure S22), and maintains porosity (Figure S23). The Ni, Mn, and Cl content of **1-Ni**, calculated by XPS (Figure S24), IC, and ICP-MS measurements, allowed a assignment of the formula of **1-Ni** as Ni<sub>3</sub>[(Mn<sub>2.6</sub>Ni<sub>1.4</sub>Cl)<sub>3</sub>(BTT)<sub>8</sub>]<sub>2</sub> whereby an average of 1.4 Mn cations are replaced by Ni in each tetrametal cluster. This assignment assumes full exchange of more labile extraframework cations. Even though the formula represents an average that allows for a mixture of clusters with varying compositions Ni<sub>x</sub>Mn<sub>4-x</sub> ( $x = 0-4$ ), the presence of Mn<sub>4</sub> clusters is ruled out by subsequent reactivity studies (vide infra). As with **1**, NiCl<sub>2</sub> equivalents can be removed from **1-Ni** by soaking it in MeOH to generate the chloride-vacant material **2-Ni** as a green crystalline solid, in the solvated state (Figure S22). In **2-Ni**, 14% of its tetranuclear clusters are chloride-deficient, as confirmed by ICP-MS, IC, and XPS analyses (Figure S25). Green crystals of **2-Ni** can be desolvated under a dynamic vacuum at 120 °C for 18 h to yield a tan, crystalline solid that retains the same structure as **2-Ni** (Figure S22). Importantly, dosing O<sub>2</sub> onto this tan solid does not result in a color change and yields no changes to the Raman spectrum (Figure S26). Notably, no new bands are observed at 607, 636, 671, or 692 cm<sup>-1</sup> which also confirms that no Mn<sub>4</sub> clusters are present in **2-Ni**. Thus, the exchange of at least one Mn ion in tetranuclear Mn<sub>4</sub> clusters by a metal with a less accessible one-electron redox couple eliminates all reactivity with O<sub>2</sub>, further confirming that reactivity occurs at the vacant Mn<sub>4</sub> cluster.

## CONCLUSIONS

Our work provides structural and functional precedent for the interconversion between O<sub>2</sub> and metal–oxos and offers insight into the four-electron cleavage and formation of O–O double bonds. A necessary caveat is that the complex electronic structure of these intermediates is challenging for DFT modeling, but we expect that the qualitative conclusions would be unchanged with either changing the DFT functional or more computationally intensive theoretical modeling. Cleavage and formation of O=O bonds typically require independent chemical systems or metalloenzyme cofactors but are achieved here in a single Mn<sub>4</sub> cluster. The results thus highlight both the utility of multinuclear clusters in mitigating the redox burden for multielectron processes and the advantage of placing such clusters inside MOFs, to lower the entropic penalty for coupling two oxo groups and favor the formation of the O–O bond, which is often the rate-determining step in O<sub>2</sub> evolution mechanisms.

## ASSOCIATED CONTENT

### Supporting Information

The Supporting Information is available free of charge at <https://pubs.acs.org/doi/10.1021/jacs.3c05374>.

Experimental; XPS spectra; Raman spectra; PXRD patterns; N<sub>2</sub> adsorption isotherms; images of single crystals; computationally optimized structures; coordinates; calculates frontier orbitals; and calculated vibration modes of clusters and intermediates (PDF)

## AUTHOR INFORMATION

### Corresponding Author

Mircea Dincă – Department of Chemistry, Massachusetts Institute of Technology, Cambridge, Massachusetts 02139, United States; [orcid.org/0000-0002-1262-1264](https://orcid.org/0000-0002-1262-1264); Email: [mdinca@mit.edu](mailto:mdinca@mit.edu)

### Authors

Xin He – Department of Chemistry, Massachusetts Institute of Technology, Cambridge, Massachusetts 02139, United States; [orcid.org/0000-0001-8461-8868](https://orcid.org/0000-0001-8461-8868)

Andrei Iliescu – Department of Chemistry, Massachusetts Institute of Technology, Cambridge, Massachusetts 02139, United States

Tzuhsung Yang – Department of Chemical Engineering, Massachusetts Institute of Technology, Cambridge, Massachusetts 02139, United States; [orcid.org/0000-0002-6751-9806](https://orcid.org/0000-0002-6751-9806)

Maxx Q. Arguilla – Department of Chemistry, Massachusetts Institute of Technology, Cambridge, Massachusetts 02139, United States; [orcid.org/0000-0001-9948-0814](https://orcid.org/0000-0001-9948-0814)

Tianyang Chen – Department of Chemistry, Massachusetts Institute of Technology, Cambridge, Massachusetts 02139, United States; [orcid.org/0000-0003-3142-8176](https://orcid.org/0000-0003-3142-8176)

Heather J. Kulik – Department of Chemical Engineering, Massachusetts Institute of Technology, Cambridge, Massachusetts 02139, United States; [orcid.org/0000-0001-9342-0191](https://orcid.org/0000-0001-9342-0191)

Complete contact information is available at: <https://pubs.acs.org/10.1021/jacs.3c05374>

### Author Contributions

<sup>§</sup>X.H. and A.I. contributed equally.

### Notes

The authors declare no competing financial interest.

## ACKNOWLEDGMENTS

Work in the Dincă lab (X.H., A.I., T.C., and M.D.) was supported by the National Science Foundation (DMR-2105495). Computational work was supported by the Inorganometallic Catalyst Design Center, an EFRC funded by the DOE, Office of Basic Energy Sciences (DE-SC0012702) to T.Y. and H.J.K. This work was carried out in part using computational resources from the Extreme Science and Engineering Discovery Environment (XSEDE), which is supported by the National Science Foundation grant number ACI-1548562. We thank C. Sun for assistance with mass spectrometry, J. Oppenheim for assistance with gas adsorption measurements, and A. Nandy for assistance with TD-DFT figures.

## REFERENCES

- (1) Kern, J.; Chatterjee, R.; Young, I. D.; Fuller, F. D.; Lassalle, L.; Ibrahim, M.; Gul, S.; Fransson, T.; Brewster, A. S.; Alonso-Mori, R.; Hussein, R.; Zhang, M.; Douthit, L.; de Lichtenberg, C.; Cheah, M. H.; Shevela, D.; Wersig, J.; Seuffert, I.; Sokaras, D.; Pastor, E.; Weninger, C.; Kroll, T.; Sierra, R. G.; Aller, P.; Butryn, A.; Orville, A. M.; Liang, M.; Batyuk, A.; Koglin, J. E.; Carbajo, S.; Boutet, S.; Moriarty, N. W.; Holton, J. M.; Dobbek, H.; Adams, P. D.; Bergmann, U.; Sauter, N. K.; Zouni, A.; Messinger, J.; Yano, J.; Yachandra, V. K. Structures of the intermediates of Kok's photosynthetic water oxidation clock. *Nature* **2018**, *563*, 421–425.
- (2) Solomon, E. I.; Augustine, A. J.; Yoon, J. O<sub>2</sub> reduction to H<sub>2</sub>O by the multicopper oxidases. *Dalton Trans.* **2008**, 3921–3932.
- (3) Kanan, M. W.; Nocera, D. G. In situ formation of an oxygen-evolving catalyst in neutral water containing phosphate and Co<sup>2+</sup>. *Science* **2008**, *321*, 1072–1075.
- (4) Pegis, M. L.; Wise, C. F.; Martin, D. J.; Mayer, J. M. Oxygen reduction by homogeneous molecular catalysts and electrocatalysts. *Chem. Rev.* **2018**, *118*, 2340–2391.
- (5) Halfen, J. A.; Mahapatra, S.; Wilkinson, E. C.; Kaderli, S.; Young, V. G., Jr.; Que, L., Jr.; Zuberbühler, A. D.; Tolman, W. B. Reversible cleavage and formation of the dioxygen O–O bond within a dicopper complex. *Science* **1996**, *271*, 1397–1400.
- (6) Betley, T. A.; Surendranath, Y.; Childress, M. V.; Alliger, G. E.; Fu, R.; Cummins, C. C.; Nocera, D. G. A ligand field chemistry of oxygen generation by the oxygen-evolving complex and synthetic active sites. *Philos. Trans. R. Soc., B* **2008**, *363*, 1293–1303.
- (7) Blakemore, J. D.; Crabtree, R. H.; Brudvig, G. W. Molecular catalysts for water oxidation. *Chem. Rev.* **2015**, *115*, 12974–13005.
- (8) Elwell, C. E.; Gagnon, N. L.; Neisen, B. D.; Dhar, D.; Spaeth, A. D.; Yee, G. M.; Tolman, W. B. Copper–oxygen complexes revisited: Structures, spectroscopy, and reactivity. *Chem. Rev.* **2017**, *117*, 2059–2107.
- (9) Adam, S. M.; Wijeratne, G. B.; Rogler, P. J.; Diaz, D. E.; Quist, D. A.; Liu, J. J.; Karlin, K. D. Synthetic Fe/Cu complexes: Toward understanding heme-copper oxidase structure and function. *Chem. Rev.* **2018**, *118*, 10840–11022.
- (10) Jasniewski, A. J.; Que, L. Dioxygen activation by nonheme diiron enzymes: Diverse dioxygen adducts, high-valent intermediates, and related model complexes. *Chem. Rev.* **2018**, *118*, 2554–2592.
- (11) Zhang, B.; Sun, L. Artificial photosynthesis: Opportunities and challenges of molecular catalysts. *Chem. Soc. Rev.* **2019**, *48*, 2216–2264.
- (12) Cole, A. P.; Root, D. E.; Mukherjee, P.; Solomon, E. I.; Stack, T. D. P. A trinuclear intermediate in the copper-mediated reduction of O<sub>2</sub>: Four electrons from three coppers. *Science* **1996**, *273*, 1848–1850.
- (13) Lionetti, D.; Day, M. W.; Agapie, T. Metal-templated ligand architectures for trinuclear chemistry: Tricopper complexes and their O<sub>2</sub> reactivity. *Chem. Sci.* **2013**, *4*, 785–790.
- (14) Cook, B. J.; Di Francesco, G. N.; Kieber-Emmons, M. T.; Murray, L. J. A tricopper(I) complex competent for O atom transfer, C–H bond activation, and multiple O<sub>2</sub> activation steps. *Inorg. Chem.* **2018**, *57*, 11361–11368.
- (15) Kanady, J. S.; Tsui, E. Y.; Day, M. W.; Agapie, T. A synthetic model of the Mn<sub>3</sub>Ca subsite of the oxygen-evolving complex in photosystem II. *Science* **2011**, *333*, 733–736.
- (16) Mukherjee, S.; Stull, J. A.; Yano, J.; Stamatatos, T. C.; Pringouri, K.; Stich, T. A.; Abboud, K. A.; Britt, R. D.; Yachandra, V. K.; Christou, G. Synthetic model of the asymmetric [Mn<sub>3</sub>CaO<sub>4</sub>] cubane core of the oxygen-evolving complex of photosystem II. *Proc. Natl. Acad. Sci. U. S. A.* **2012**, *109*, 2257–2262.
- (17) Zhang, C.; Chen, C.; Dong, H.; Shen, J.-R.; Dau, H.; Zhao, J. A synthetic Mn<sub>4</sub>Ca-cluster mimicking the oxygen-evolving center of photosynthesis. *Science* **2015**, *348*, 690–693.
- (18) Maayan, G.; Gluz, N.; Christou, G. A bioinspired soluble manganese cluster as a water oxidation electrocatalyst with low overpotential. *Nat. Catal.* **2018**, *1*, 48–54.
- (19) Dismukes, G. C.; Brimblecombe, R.; Felton, G. A. N.; Pryadun, R. S.; Sheats, J. E.; Spiccia, L.; Swiegers, G. F. Development of bioinspired Mn<sub>4</sub>O<sub>4</sub>-cubane water oxidation catalysts: Lessons from photosynthesis. *Acc. Chem. Res.* **2009**, *42*, 1935–1943.
- (20) Collman, J. P.; Devaraj, N. K.; Decréau, R. A.; Yang, Y.; Yan, Y.-L.; Ebina, W.; Eberspacher, T. A.; Chidsey, C. E. D. A cytochrome C



oxidase model catalyzes oxygen to water reduction under rate-limiting electron flux. *Science* **2007**, *315*, 1565–1568.

(21) Powers, T. M.; Betley, T. A. Testing the polynuclear hypothesis: Multielectron reduction of small molecules by triiron reaction sites. *J. Am. Chem. Soc.* **2013**, *135*, 12289–12296.

(22) DeRosha, D. E.; Chilkuri, V. G.; Van Stappen, C.; Bill, E.; Mercado, B. Q.; DeBeer, S.; Neese, F.; Holland, P. L. Planar three-coordinate iron sulfide in a synthetic [4Fe-3S] cluster with biomimetic reactivity. *Nat. Chem.* **2019**, *11*, 1019–1025.

(23) Yaghi, O. M.; Kalmutzki, M. J.; Diercks, C. S. *Introduction to reticular chemistry: Metal-organic frameworks and covalent organic frameworks*; Wiley-VCH, 2019.

(24) Dincă, M.; Dailly, A.; Liu, Y.; Brown, C. M.; Neumann, D. A.; Long, J. R. Hydrogen storage in a microporous metal-organic framework with exposed Mn<sup>2+</sup> coordination sites. *J. Am. Chem. Soc.* **2006**, *128*, 16876–16883.

(25) Shook, R. L.; Gunderson, W. A.; Greaves, J.; Ziller, J. W.; Hendrich, M. P.; Borovik, A. S. A monomeric Mn<sup>III</sup>-peroxo complex derived directly from dioxygen. *J. Am. Chem. Soc.* **2008**, *130*, 8888–8889.

(26) Liu, L.-L.; Li, H.-X.; Wan, L.-M.; Ren, Z.-G.; Wang, H.-F.; Lang, J.-P. A Mn(III)-superoxo complex of a zwitterionic calix[4]-arene with an unprecedented linear end-on Mn(III)-O<sub>2</sub> arrangement and good catalytic performance for alkene epoxidation. *Chem. Commun.* **2011**, *47*, 11146–11148.

(27) Coggins, M. K.; Sun, X.; Kwak, Y.; Solomon, E. I.; Rybak-Akimova, E.; Kovacs, J. A. Characterization of metastable intermediates formed in the reaction between a Mn(II) complex and dioxygen, including a crystallographic structure of a binuclear Mn(III)-peroxo species. *J. Am. Chem. Soc.* **2013**, *135*, 5631–5640.

(28) Limburg, J.; Vrettos, J. S.; Chen, H.; de Paula, J. C.; Crabtree, R. H.; Brudvig, G. W. Characterization of the O<sub>2</sub>-evolving reaction catalyzed by [(terpy)(H<sub>2</sub>O)Mn<sup>III</sup>(O)<sub>2</sub>Mn<sup>IV</sup>(OH<sub>2</sub>)(terpy)](NO<sub>3</sub>)<sub>3</sub> (terpy = 2,2':6,2''-terpyridine). *J. Am. Chem. Soc.* **2001**, *123*, 423–430.

(29) Hong, S.; Sutherlin, K. D.; Park, J.; Kwon, E.; Siegler, M. A.; Solomon, E. I.; Nam, W. Crystallographic and spectroscopic characterization and reactivities of a mononuclear non-haem iron(III)-superoxo complex. *Nat. Commun.* **2014**, *5*, 5440.

(30) Brozek, C. K.; Cozzolino, A. F.; Teat, S. J.; Chen, Y.-S.; Dincă, M. Quantification of site-specific cation exchange in metal-organic frameworks using multi-wavelength anomalous X-ray dispersion. *Chem. Mater.* **2013**, *25*, 2998–3002.

(31) Dincă, M.; Long, J. R. High-enthalpy hydrogen adsorption in cation-exchanged variants of the microporous metal-organic framework Mn<sub>3</sub>[(Mn<sub>4</sub>Cl)<sub>3</sub>(BTT)<sub>8</sub>(CH<sub>3</sub>OH)<sub>10</sub>]<sub>2</sub>. *J. Am. Chem. Soc.* **2007**, *129*, 11172–11176.